Geophysical Research Letters

Supporting Information for

Cloud-to-ground lightning and near-surface fire weather control wildfire occurrence in Arctic tundra

Jiaying He[1,2], Tatiana V. Loboda[2], Dong Chen[2], and Nancy H. F. French[3]

[1]Department of Earth System Science, Ministry of Education Key Laboratory for Earth System Modeling, Institute for Global Change Studies, Tsinghua University, Beijing 100084, China.

[2]Department of Geographical Sciences, University of Maryland, College Park, MD 20742, US.

[3]Michigan Technological Research Institute, Michigan Technological University, Ann Arbor, MI 48105, US.

Contents of this file

Text S1
Figures S1 to S6
Tables S1 to S3

Introduction

This file includes one supplementary text, six supplementary figures and three supplementary tables. Text S1 provides additional descriptions about how we determined the dates and locations of fire events in Section 2.2.1. Figures S1 – S2 include supporting information of the methodology. Figures S3 – S5 and Tables S1 – S3 provide additional details of the results.

Text S1.

Locations of tundra fire occurrences from 2001 to 2019 were determined using the 1km MODIS Thermal Anomalies/Fire locations – Collection 6 data product (MCD14ML V6; Giglio et al., 2016) obtained from NASA's Fire Information for Resource Management System (FIRMS). Since fires have strong emission of mid-infrared radiation, this active fire product detects fires based on brightness temperatures from MODIS 4- and 11-μm bands using a contextual algorithm (Giglio et al., 2003). In addition to coordinates (latitude and longitude) of active fire points, attributes including brightness temperature, acquisition date, acquisition time, fire radiative power, and detection confidence are also recorded in this data product. Here we only considered active fire points classified as nominal or high confidence levels (detection confidence above 30%) for further data processing and analyses.

We first extracted MODIS active fire points in the tundra using a 10km buffered boundary of the Circumpolar Arctic Vegetation Map (CAVM; Walker et al., 2005). We designed a clustering method based on the Density-Based Spatial Clustering of Applications with Noise (DBSCAN; Ester et al., 1996) algorithm to identify the tundra fire clusters (Figure S1). The DBSCAN algorithm separates points of high density from those of low density and locates these regions as clusters. The ε parameter in DBSCAN represents the maximum distance between two neighboring points. Here we set the ε parameter to 2.5 km, as suggested by the study of Loboda and Csiszar (2007). For each year, we applied the DBSCAN algorithm to the tundra fire points for each year. Since fires occurring at different times could be grouped into the same cluster considering their spatial proximity, we then examined the temporal gap (Gap_{time}) among all active fire points grouped in each cluster. The temporal gap was determined as 4 days (*minDay*) to separate different fires in a certain spatial cluster, as suggested by Loboda and Csiszar (2007). The active fire points with the earliest acquisition time were then extracted as the fire occurrence locations. Finally, we removed the points outside the Arctic tundra extent as defined by the CAVM.

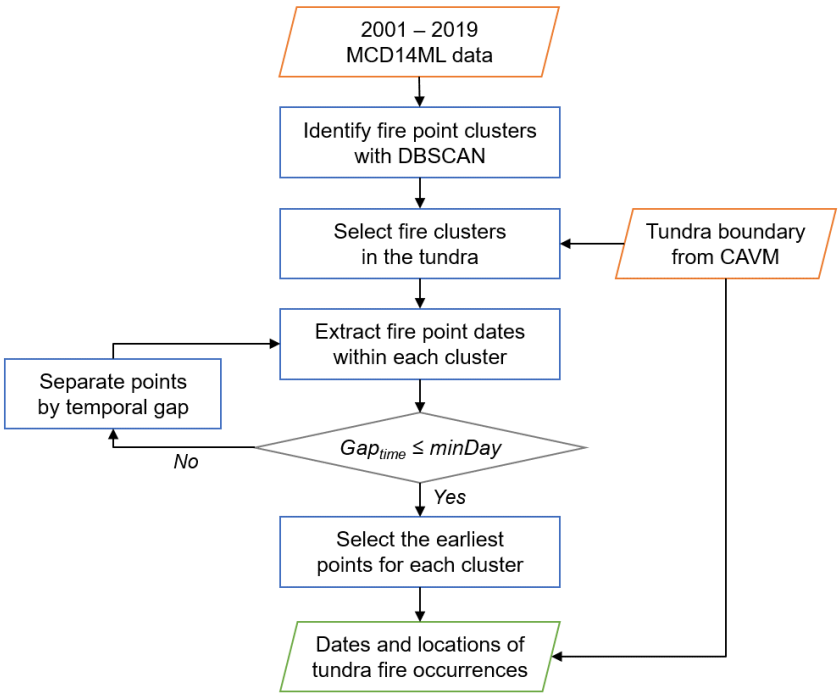

Figure S1. Workflow of determining the dates and locations of tundra fire occurrences.

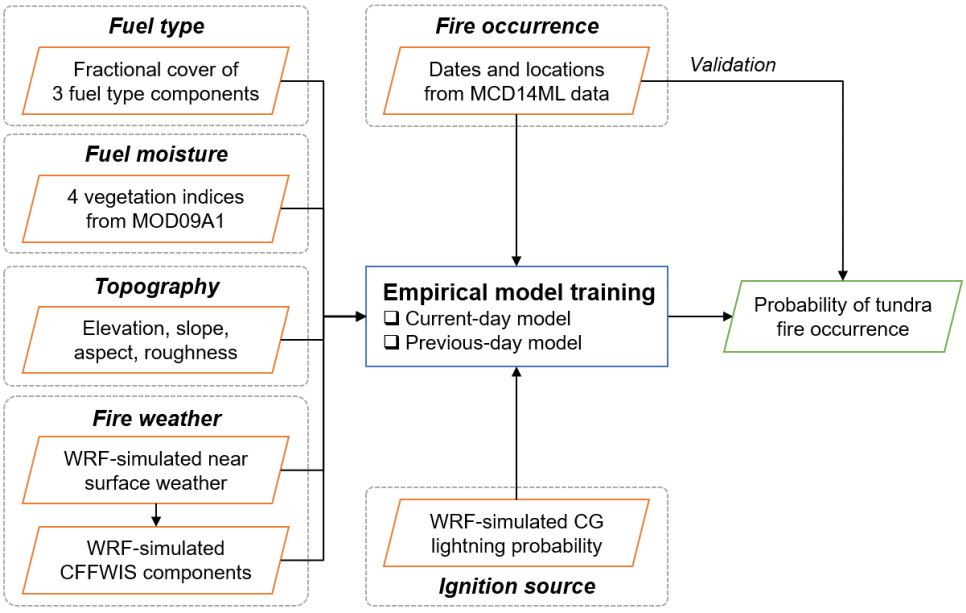

Figure S2. Methodology framework of modeling fire occurrence probability.

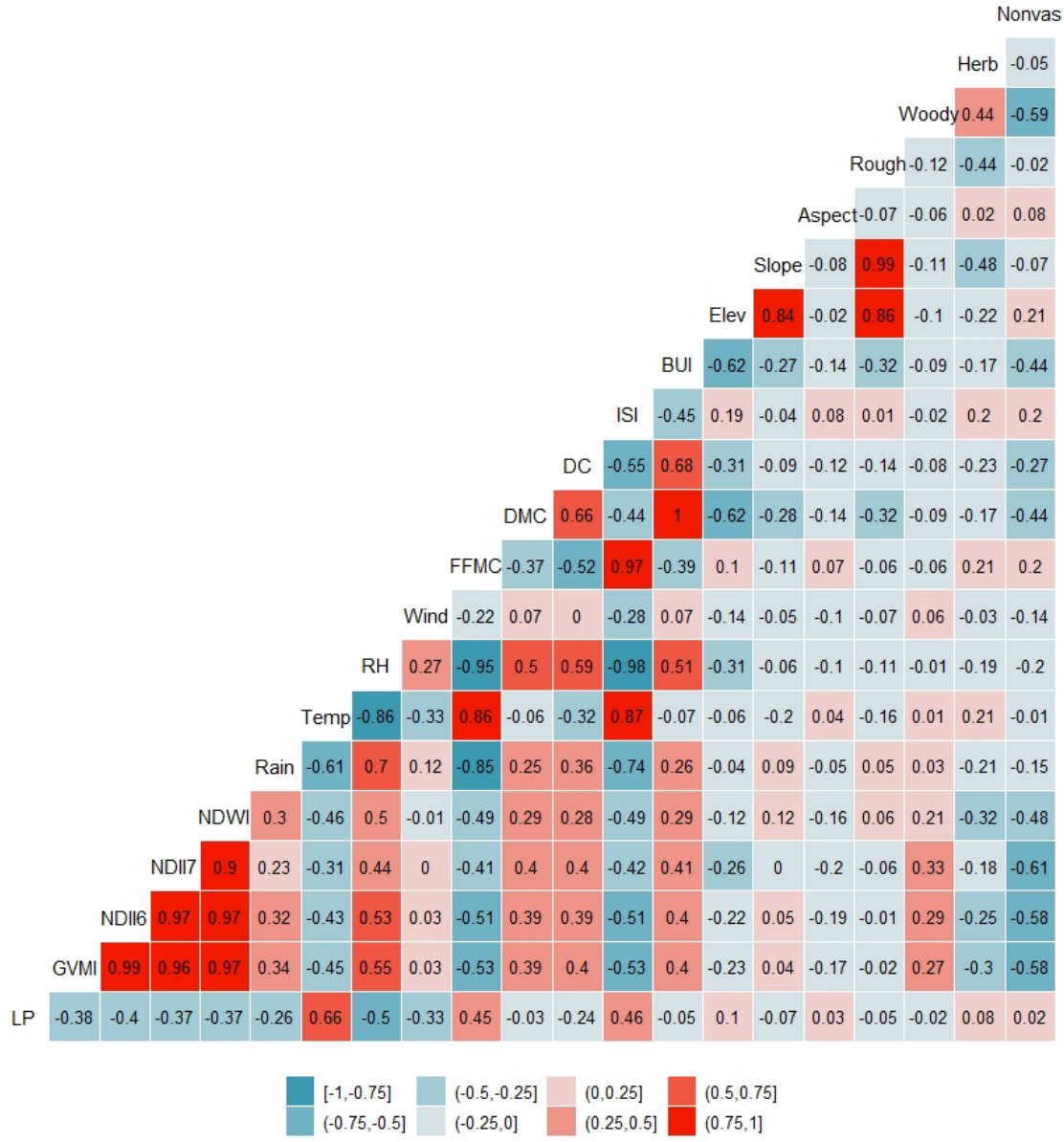

Figure S3. Correlation matrix of all variables extracted on fire-occurrence days, where "LP" represents CG lightning probability, "Temp" represents air temperature, "Elev" represents elevation, "Rough" represents roughness, "Herb" represents fractional cover of herbaceous fuel component, and "Nonvas" represents fractional cover of nonvascular fuel component.

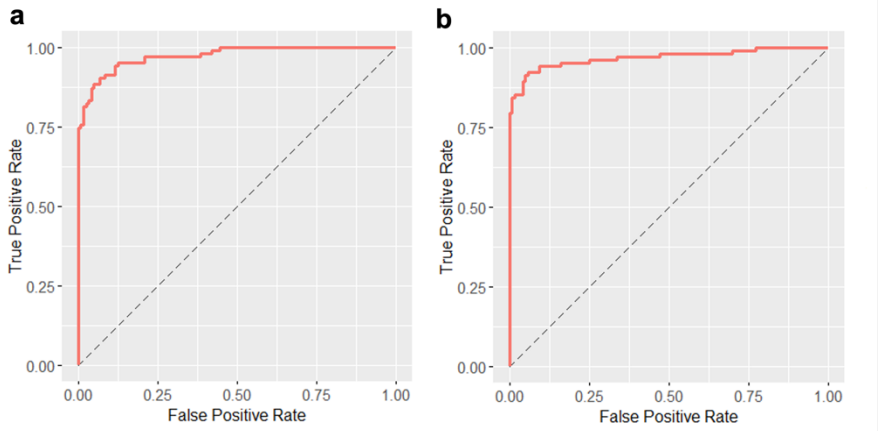

Figure S4. Receiver Operating Characteristic (ROC) curves of the two random forest (RF) models: (a) Current-day model and (b) Previous-day model.

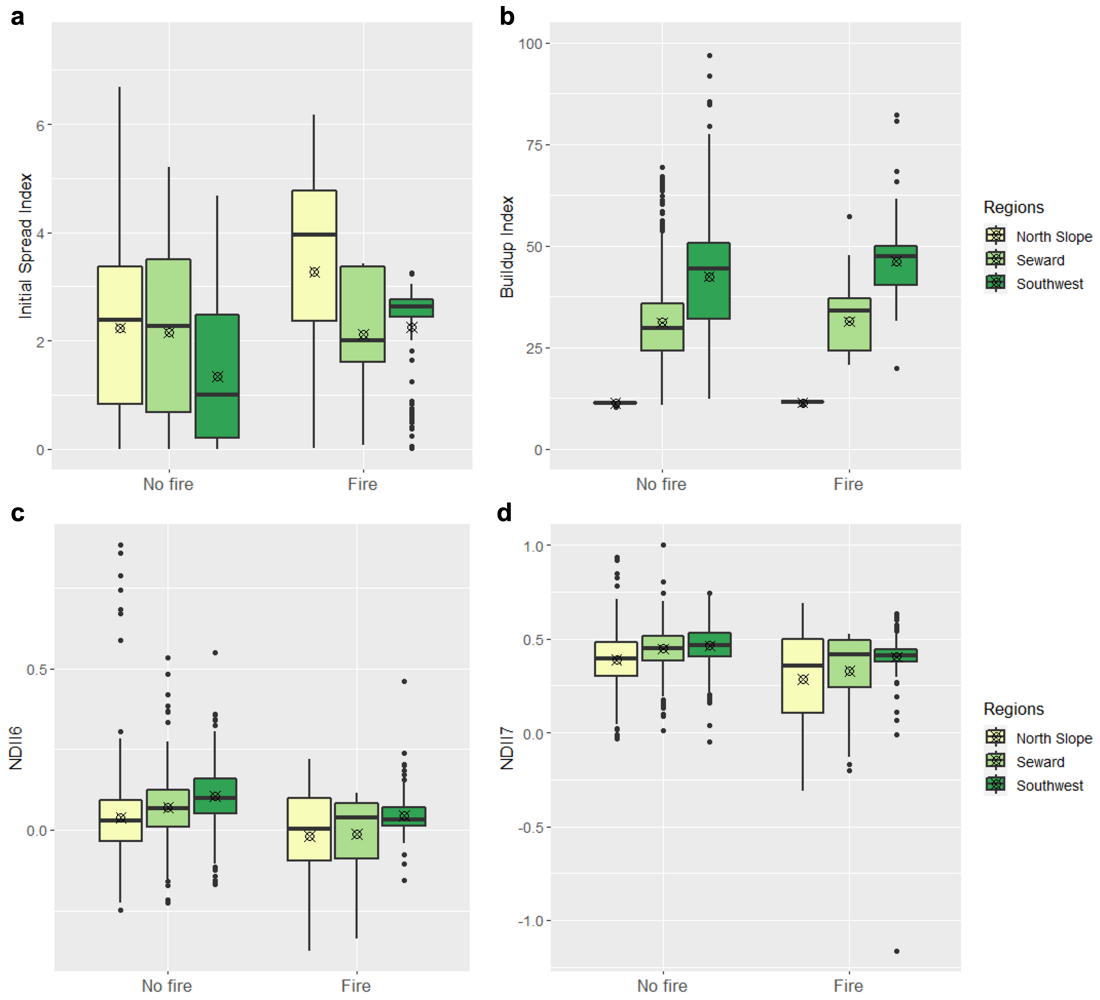

Figure S5. Boxplots showing (a) ISI, (b) BUI, (c) $NDII_6$, and (d) $NDII_7$ of "Fire" and "No fire" events across the three major tundra regions.

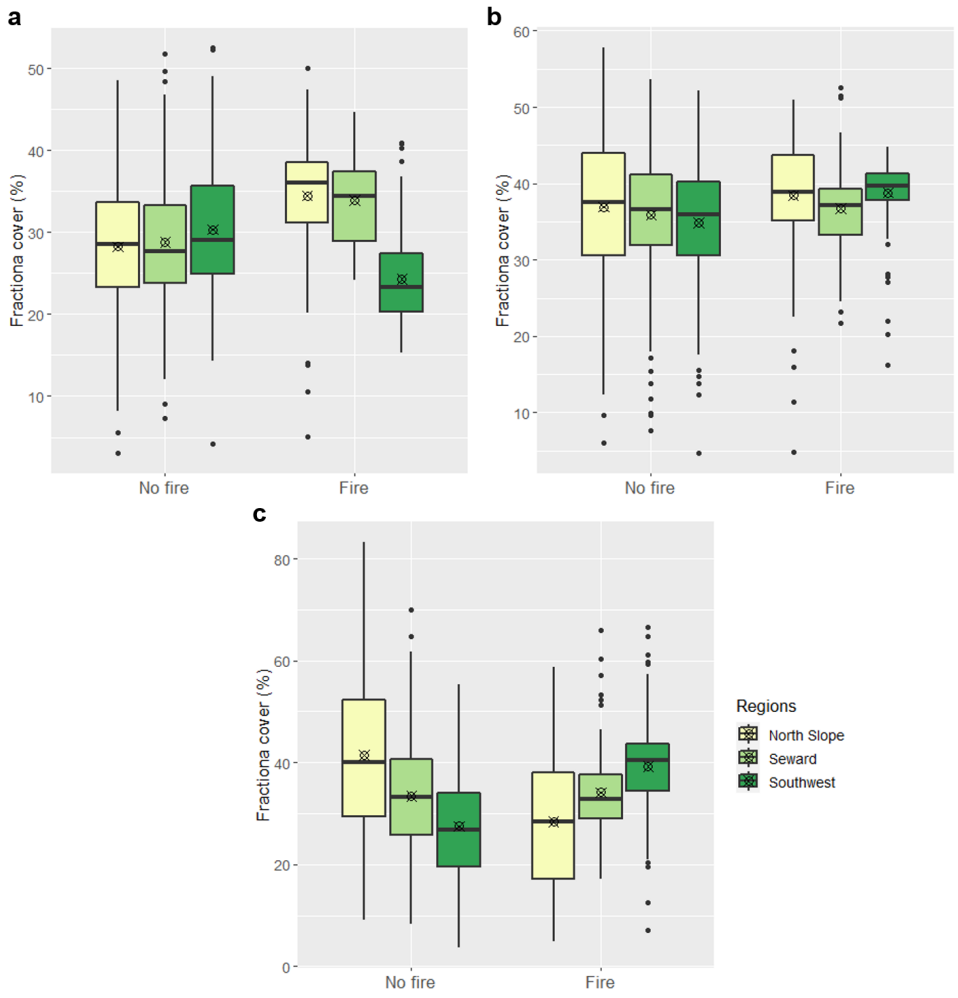

Figure S6. Boxplots showing the fractional cover of (a) woody, (b) herbaceous, and (c) nonvascular fuel components of "Fire" and "No fire" events from the exact dates of fire occurrences across the three major tundra regions.

Vegetation index	Formula with MODIS bands	Reference
Normalized Difference Infrared Index ($NDII_6$)	$\frac{\rho_2 - \rho_6}{\rho_2 + \rho_6}$	(Hardisky et al., 1983)
Normalized Difference Infrared Index ($NDII_7$)	$\frac{\rho_2 - \rho_7}{\rho_2 + \rho_7}$	(Hardisky et al., 1983)
Normalized Difference Water Index (NDWI)	$\frac{\rho_2 - \rho_5}{\rho_2 + \rho_5}$	(Gao, 1996)
Global Vegetation Moisture Index (GVMI)	$\frac{(\rho_2 + 0.1) - (\rho_6 + 0.02)}{(\rho_2 + 0.1) + (\rho_6 + 0.02)}$	(Ceccato et al., 2002)

Table S1. Vegetation indices for estimating live fuel moisture content with MODIS bands.

Severity	Fire season	Fire event count	Fire event dates
Light	2002	12	5/23, 6/3, 6/18, 7/10, 7/20, 7/28, 8/2, 8/5, 8/15, 8/22, 9/22
	2006	3	5/31, 7/7
	2008	5	6/4, 6/5, 6/7, 6/8, 6/13
	2013	11	5/31, 6/5, 6/20, 6/21, 7/11, 7/30
	2017	12	6/6, 6/7, 6/8, 6/16, 6/19, 6/28
Moderate	2007	23	6/4, 6/10, 7/5, 7/6, 7/7, 7/12, 7/14, 7/16, 7/17, 8/2/2007, 8/29/2007, 9/8/2007, 9/9, 9/19, 9/30
	2010	27	6/1, 6/8, 6/9, 6/21, 6/22, 6/23, 6/24, 7/1, 7/2, 7/3, 7/4, 7/8, 7/10
Severe	2015	49	6/1, 6/2, 6/16, 6/20, 6/21, 6/22, 6/23, 6/24, 6/25, 6/29, 6/30, 7/2, 7/3, 7/4, 7/6, 7/7, 7/13, 7/14, 7/20, 7/24/2015, 7/25/2015, 8/1, 8/6

Table S2. Full list of fire occurrence dates detected from the sampled fire seasons.

(a) Current-day model				
Confusion matrix		Predictions		Class error
		No fire	Fire	
Observations	No fire	263	14	0.0505
	Fire	17	220	0.0717
(b) Previous-day model				
Confusion matrix		Predictions		Class error
		No fire	Fire	
Observations	No fire	258	19	0.0686
	Fire	26	211	0.1097

Table S3. RF results of the two models for predicting tundra fire occurrences.

Variables	North Slope		Seward Peninsula		Southwest Alaska	
	t	p-value	t	p-value	t	p-value
Lightning (current)	-6.603	<0.001***	-5.113	<0.001***	-16.18	<0.001***
Lightning (previous)	-2.337	0.030*	-5.161	<0.001***	-6.414	<0.001***
Temperature (current)	-4.789	<0.001***	-1.142	0.259	-16.59	<0.001***
Temperature (previous)	-4.726	<0.001***	-2.410	0.019*	-10.79	<0.001***
RH (current)	2.985	0.006**	0.819	0.416	9.192	<0.001***
RH (previous)	3.844	<0.001***	2.549	0.013*	7.451	<0.001***
Rain (current)	-0.132	0.896	4.487	<0.001***	3.755	<0.001**
Rain (previous)	2.215	0.030*	-0.098	0.923	4.461	<0.001***
Wind speed (current)	0.836	0.412	-2.941	0.005**	4.198	<0.001***
Wind speed (previous)	2.385	0.025*	1.989	0.052†	3.523	<0.001**
FFMC (current)	-4.321	<0.001***	-1.571	0.122	-9.433	<0.001***
FFMC (previous)	-9.820	<0.001***	-0.021	0.984	-8.876	<0.001***
DMC (current)	-5.344	<0.001***	-0.305	0.762	-3.873	<0.001***
DMC (previous)	-6.807	<0.001***	-0.280	0.780	-3.375	<0.001***
DC (current)	-3.446	<0.001***	1.705	0.093†	0.601	0.548
DC (previous)	-3.345	0.001**	1.711	0.092†	0.735	0.463
ISI (current)	-6.010	<0.001***	0.162	0.872	-9.587	<0.001***
ISI (previous)	-6.497	<0.001***	0.341	0.734	-8.502	<0.001***
BUI (current)	-3.807	<0.001***	-0.138	0.891	-3.471	<0.001***
BUI (previous)	-3.664	<0.001***	-0.113	0.911	-3.014	0.003**
GVMI	2.124	0.035*	3.879	<0.001***	8.981	<0.001***
NDII6	4.043	<0.001***	3.916	<0.001***	8.002	<0.001***
NDII7	4.423	<0.001***	3.444	0.001**	4.552	<0.001***
NDWI	3.111	0.002**	3.278	0.002**	5.414	<0.001***
Elevation	2.633	0.009**	0.749	0.457	-0.711	0.478
Slope	2.200	0.029*	3.679	<0.001***	3.394	<0.001***
Aspect	-2.903	0.004**	-1.017	0.315	2.832	0.005*
Roughness	2.947	0.004**	4.056	<0.001***	3.394	<0.001***
Woody cover	-8.689	<0.001***	-5.661	<0.001***	9.818	<0.001***
Herbaceous cover	-1.810	0.072†	-0.879	0.384	-7.148	<0.001***
Nonvascular cover	9.525	<0.001***	-0.441	0.661	-13.08	<0.001***

Table S4. Welch t-test results across different tundra regions. Significance levels of t-test results: ***p<0.001, **p<0.01, *p<0.05, and †p < 0.1.

References

Ceccato, P., Flasse, S., Grégoire, J.M., 2002. Designing a spectral index to estimate vegetation water content from remote sensing data: Part 1: Theoretical approach. Remote Sens. Environ. 82, 188–197.

Ester, M., Kriegel, H.-P., Sander, J., Xu, X., 1996. A density-based algorithm for discovering clusters in large spatial databases with noise., in: Kdd. pp. 226–231.

Gao, B., 1996. NDWI – A Normalized Difference Water Index for Remote Sensing of Vegetation Liquid Water from Space. Remote Sens. Environ. 58, 257.

Giglio, L., Descloitres, J., Justice, C.O., Kaufman, Y.J., 2003. An Enhanced Contextual Fire Detection Algorithm for MODIS. Remote Sens. Environ. 87, 273–282.

Giglio, L., Schroeder, W., Justice, C.O., 2016. The collection 6 MODIS active fire detection algorithm and fire products. Remote Sens. Environ. 178, 31–41.

Hardisky, M.A., Klemas, V., Smart, R.M., 1983. The influence of soil salinity, growth form, and leaf moisture on the spectral radiance of Spartina alterniflora canopies. Photogramm. Eng. Remote Sens. 49, 77–83.

Loboda, T. V, Csiszar, I.A., 2007. Reconstruction of fire spread within wildland fire events in Northern Eurasia from the MODIS active fire product. Glob. Planet. Change 56, 258–273.

Walker, D.A., Raynolds, M.K., Daniëls, F.J.A., Einarsson, E., Elvebakk, A., Gould, W.A., Katenin, A.E., Kholod, S.S., Markon, C.J., Melnikov, E.S., Moskalenko, N.G., Talbot, S.S., Yurtsev, B.A., Team, the other members of the C., 2005. The Circumpolar Arctic vegetation map. J. Veg. Sci. 16, 267–282.